ELSEVIER

NeuroImage

www.elsevier.com/locate/ynimg
NeuroImage 34 (2007) 1416–1427

Temporal classification of multichannel near-infrared spectroscopy signals of motor imagery for developing a brain–computer interface

Ranganatha Sitaram,[a,b,*] Haihong Zhang,[a] Cuntai Guan,[a] Manoj Thulasidas,[a] Yoko Hoshi,[c] Akihiro Ishikawa,[e] Koji Shimizu,[e] and Niels Birbaumer[b,d]

[a]*Institute for Infocomm Research, Singapore*
[b]*Institute of Medical Psychology and Behavioral Neurobiology, Eberhard-Karls-University of Tübingen, Tuebingen, Germany*
[c]*Tokyo Institute of Psychiatry, Tokyo, Japan*
[d]*National Institute of Health (NIH), Human Cortical Physiology, Bethesda, USA*
[e]*Shimadzu Corporation, Medical Systems Division, Japan*

Received 20 February 2006; revised 30 October 2006; accepted 3 November 2006
Available online 28 December 2006

There has been an increase in research interest for brain–computer interface (BCI) technology as an alternate mode of communication and environmental control for the disabled, such as patients suffering from amyotrophic lateral sclerosis (ALS), brainstem stroke and spinal cord injury. Disabled patients with appropriate physical care and cognitive ability to communicate with their social environment continue to live with a reasonable quality of life over extended periods of time. Near-infrared spectroscopy is a non-invasive technique which utilizes light in the near-infrared range (700 to 1000 nm) to determine cerebral oxygenation, blood flow and metabolic status of localized regions of the brain. In this paper, we describe a study conducted to test the feasibility of using multichannel NIRS in the development of a BCI. We used a continuous wave 20-channel NIRS system over the motor cortex of 5 healthy volunteers to measure oxygenated and deoxygenated hemoglobin changes during left-hand and right-hand motor imagery. We present results of signal analysis indicating that there exist distinct patterns of hemodynamic responses which could be utilized in a pattern classifier towards developing a BCI. We applied two different pattern recognition algorithms separately, Support Vector Machines (SVM) and Hidden Markov Model (HMM), to classify the data offline. SVM classified left-hand imagery from right-hand imagery with an average accuracy of 73% for all volunteers, while HMM performed better with an average accuracy of 89%. Our results indicate potential application of NIRS in the development of BCIs. We also discuss here future extension of our system to develop a word speller application based on a cursor control paradigm incorporating online pattern classification of single-trial NIRS data.

Index terms: Brain–computer interface (BCI); Near-infrared spectroscopy (NIRS); Amyotrophic lateral sclerosis (ALS); Motor Imagery; Support Vector Machine (SVM); Hidden Markov Model (HMM).

* Corresponding author. Institute of Medical Psychology and Behavioural Neurobiology, Eberhard-Karls-University of Tübingen, Gartenstr. 29, D-72074 Tuebingen, Germany. Fax: +49 7071 295956.
E-mail address: sitaram.ranganatha@uni-tuebingen.de (R. Sitaram).
Available online on ScienceDirect (www.sciencedirect.com).

1053-8119/$ - see front matter © 2006 Elsevier Inc. All rights reserved.
doi:10.1016/j.neuroimage.2006.11.005

Introduction

BCI can provide an alternative communication channel and environmental control capability to severely disabled persons. The quality of life depends on the possibility to communicate with the social environment. Disabled patients with appropriate physical care, and cognitive ability to communicate with a BCI, can continue to live with a reasonable quality of life over extended periods of time (Wolpaw et al., 2000a).

Brain–computer interfaces have been developed with surface electroencephalogram (EEG), electrocorticogram (ECoG) and implanted electrodes (Birbaumer et al., 1999, 2000, 2003; Birbaumer, 2006; Wolpaw, 2004; Wolpaw et al., 2000b, 2002, 2006; Wolpaw and McFarland, 2004; Serruya et al., 2002). Surface EEG has many advantages: it is non-invasive, technically less demanding, and widely available at low cost. It has a long history of usage, and its mechanisms are well known. However, EEG has certain disadvantages: long-term application and fixation of electrodes are difficult, portable devices are artifact prone, and it has low spatial resolution. Other non-invasive methods of monitoring brain activity, such as magnetoencephalography (MEG), positron emission tomography (PET) and functional magnetic resonance imaging (fMRI) could in principle provide the basis for a BCI (Weiskopf et al., 2003, 2004a, 2004b). They are, however, technically demanding and expensive. More recently, a non-invasive optical method called near-infrared spectroscopy (NIRS) promises flexibility of use, portability, metabolic specificity, good spatial resolution, localized information, high sensitivity in detecting small substance concentrations and affordability (Villringer and Obrig, 2002). NIRS has no doubt certain disadvantages. It is slow to operate because of the inherent latency of the hemodynamic response. The signal strength is affected by hair on the head. Furthermore, relative motion of the optodes on the hair may introduce motion artifacts and drifts in the hemodynamic signal. Nevertheless, NIRS' ability to record localized brain activity with a

spatial resolution in the order of centimeter (depending on the probe geometry) provides us with an excellent opportunity to control a variety of motor and cognitive activities in a BCI.

The main goal of the present study was to ascertain the feasibility of using near-infrared spectroscopy for developing a BCI. We chose motor imagery of left-hand and right-hand as the paradigm of BCI control as it has been shown to work well in previous research on EEG-based BCIs (Pfurtscheller et al., 1998, 2000). Our objective was to develop a viable set of methods for offline processing and classification of NIRS data, with the intention of incorporating them later on in an online BCI. To this end, we explored the use of two pattern recognition techniques, Support Vector Machines (SVM) and Hidden Markov Model (HMM), for classifying NIRS signals.

The present NIRS–BCI system incorporates the continuous wave technique of near-infrared spectroscopy. Regional brain activation is accompanied by increases in regional cerebral blood flow (rCBF) and the regional cerebral oxygen metabolic rate ($rCMRO_2$) (Villringer and Obrig, 2002). The degree of increases in rCBF exceeds that of increases in $rCMRO_2$ resulting in a decrease in deoxygenated hemoglobin in venous blood. Thus, increase in total hemoglobin and oxygenated hemoglobin with a decrease in deoxygenated hemoglobin is expected to be observed in activated areas during NIRS measurement. The continuous wave approach uses multiple pairs or channels of light sources and light detectors operating at 2 or more discrete wavelengths. The light source may be a laser or a light emitting diode (LED). The optical parameter measured is attenuation of light intensity due to absorption by the intermediate tissue. The concentration changes of oxygenated hemoglobin and deoxygenated hemoglobin are computed from the changes in the light intensity at different wavelengths, using the modified Beer–Lambert equation (Villringer and Obrig, 2002). The advantage of the continuous wave approach is its simplicity, flexibility and high signal-to-noise ratio. The depth of brain tissue which can be measured from the surface is typically 1–3 cm.

It has been shown in electrophysiological studies (Beisteiner et al., 1995) that brain activation during motor imagery is similar to the activation during actual execution of movement. In this study, changes of DC potentials between task execution and imagination were localized in the central scalp regions (C3, Cz, C4) with larger amplitudes during execution of the task than when only imagining to do so. Primary motor cortex was active in both the tasks. Benaron et al. (2000) demonstrated optical response resulting in the contralateral hemisphere around 5–8 s after the onset of movement. Sitaram et al. (2005) and Coyle et al. (2004) reported similar optical response using NIRS signals during overt and covert hand movements. Pfurtscheller et al. (1998, 2000, 2006) reported a direct EEG-based BCI using motor imagery. It is important that, for a BCI to be user-friendly, the mental task should be easy to learn. With this view and based on the above findings, we chose motor imagery as the basis for our BCI. The BCI would operate by classifying the time series of oxygenated hemoglobin and deoxygenated hemoglobin at multiple channels of the NIRS system into left-hand and right-hand imagery.

We applied two different pattern recognition techniques, SVM and HMM, to the classification problem. SVMs are learning systems developed by Vapnik (1998). SVM has been demonstrated to work well in a number of real-world applications including BCI (Blankertz et al., 2001). A Markov model is a finite state machine which can be used to model a time series. HMMs were first successfully applied for speech recognition, and later in molecular biology for modeling the probabilistic profile of protein families (Rabiner, 1989). HMM has been successfully used in a BCI application for online classification of EEG signals acquired during left-hand and right-hand motor imagery (Obermaier et al., 1999). To our knowledge, this is the first time that SVM and HMM techniques have been used to classify NIRS signals for the development of a BCI.

In this paper, we describe the experimental paradigm of motor imagery; method of signal acquisition; preliminary signal analysis to test whether there are significant patterns in the hemodynamic response to motor imagery; offline classification of the NIRS signal using two classification techniques (SVM and HMM); and finally the results of signal processing, analysis and classification. We end with a discussion of the application of these techniques to the online classification problem towards developing a NIRS–BCI system.

Materials and methods

Subjects

Five healthy subjects (3 males and 2 females, mean age = 30) voluntarily participated in the study. None of the recruited subjects had neurological or psychiatric history or was on medication. Each of them gave written informed consent for the experiment. The experiment was approved by the Ethical Committee of the Tokyo Institute of Psychiatry, Japan.

Experimental procedure

NIRS signals were collected from each subject performing both overt motor execution (finger tapping) and covert motor imagery with left-hand and right-hand. Fig. 1(a) shows the schematic diagram of the protocol. During the experiment, the subject sat on a chair in a quiet room in front of a computer screen which displayed the stimuli. A single trial comprised of a baseline block, a preparation block and a motor task block, in that order. Each trial started with a baseline block during which the subject fixated on the cross displayed on the screen for 8 s. This was followed by a beep indicating the subject to get ready for the motor task. The preparation phase lasted for 2 s. Following this, the subject performed the motor task as indicated on the screen for a period of 10 s. The type of motor task to be performed was indicated by the text on the computer screen—'LEFT' for left-hand motor task and 'RIGHT' for right-hand task. During the finger tapping task, subjects performed 3–4 numbers of self-paced tapping of fingers of the specified hand within the 10 s duration of the task. During the motor imagery task, subjects performed equal number of self-paced imagination of finger tapping.

Data for finger tapping and imagery were collected in two separate sessions. Each of left-hand and right-hand tasks for finger tapping and imagery was carried out for totally 80 trials, in four blocks of 20 trials each, with a rest period of 2 min between blocks.

Signal acquisition

We used a multichannel NIRS instrument (OMM-1000 from Shimadzu Corporation, Japan) for acquiring oxygenated hemoglobin and deoxygenated hemoglobin concentration changes during motor imagery. The system operated at three different wavelengths

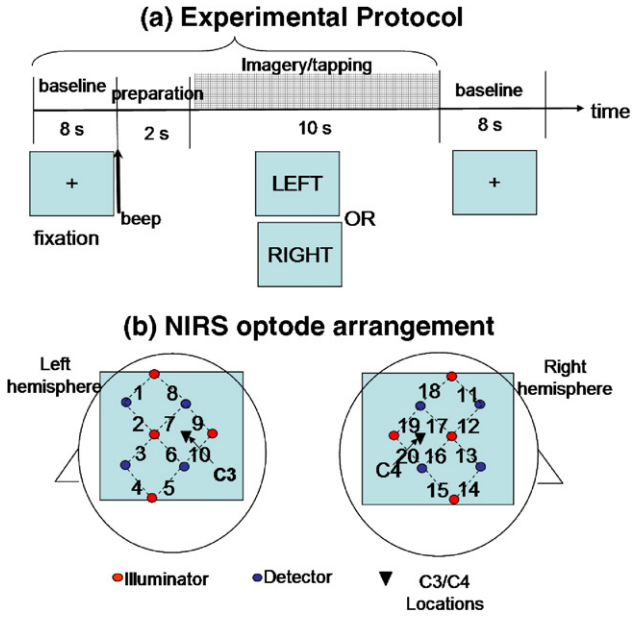

Fig. 1. (a) Experimental paradigm for finger tapping and motor imagery for collecting NIRS signals from subjects. Each trial consisted of a baseline block of 8 s, a preparation block of 2 s and motor task block of 10 s. Finger tapping and motor imagery data were collected in separate sessions. The type of task (left or right hand) was specified on the computer screen in a pseudo-random manner. During the task, subjects performed 3–4 numbers of self-paced overt execution or imagination (as specified) of finger tapping of the specified hand within the 10 s duration of the task. (b) Multichannel NIRS optode arrangement on the scalp. The optodes were arranged on the left and right hemisphere on the subject's head, above the motor cortex, around C3 (left hemisphere) and C4 (right hemisphere) areas (International 10–20 System). A pair of illuminator and detector optodes formed one channel. Four illuminators and four detectors in the arrangement resulted in 10 channels.

of 780 nm, 805 nm and 830 nm, emitting an average power of 3 mW mm^{-2}.

The illuminator and detector optodes were placed on the scalp. The detector optodes were fixed at a distance of 3 cm from the illuminator optodes. The optodes were arranged on the left and right hemisphere on the subject's head, above the motor cortex, around C3 (left hemisphere) and C4 (right hemisphere) areas (International 10–20 System). A pair of illuminator and detector optodes formed one channel. Four illuminators and four detectors in the arrangement resulted in 10 channels on each hemisphere, as shown by the dashed lines in the Fig. 1(b). Near-infrared rays leave each illuminator, pass through the skull and the brain tissue of the cortex and are received by the detector optodes. The photomultiplier cycles through all the illuminator–detector pairings to acquire data at every sampling period. The data were acquired at a sampling rate of 14 Hz and digitized by the 16-bit analog to digital converter.

The NIRS instrument was capable of storing the raw signal intensity values for each of the 3 wavelengths, the stimuli codes (1 for left-hand task and 2 for right-hand task) as well as the derived values of oxygenated and deoxygenated hemoglobin concentration changes for all time points in an output file in a pre-specified format. The signal preprocessing, analysis and classification programs were implemented to read the data from the file either in an offline mode or in an online mode.

Preliminary signal analysis

Our objective, in carrying out this preliminary analysis, was to observe the responses of oxygenated hemoglobin and deoxygenated hemoglobin at different channels on both hemispheres due to left-hand and right-hand imagery tasks. The intention was to check if there were significant patterns or trends in the data. Offline analysis was performed using a custom Matlab NIRS data analysis program (HomER version 4.0, available for public download and use at http://www.nmr.mgh.harvard.edu/PMI/). A caveat was that the HomER toolkit accepted only the raw intensity data as input to compute the oxygenated hemoglobin and deoxygenated hemoglobin concentration changes using the modified Beer–Lambert equation (Delpy et al., 1988). For this reason, we could not use the hemoglobin concentration changes obtained from the NIRS instrument directly in this analysis.

Preprocessing started with the raw intensity data from all channels being normalized to compute a relative (percent) change by dividing each value by the mean of the data.

$$\text{Norm Intensity}(t) = \text{Intensity}(t)/\text{Mean Intensity}.$$

The intensity normalized data were then low-pass-filtered using the Chebyshev type II filter of order 3 with a cut-off frequency of 0.7 Hz and pass-band (ripple) attenuation 0.5 dB. After filtering, a value of 1.0 was added to make the mean of the data equal to unity. The change in optical density, called delta-optical density, was then calculated for each wavelength as the negative logarithm of the normalized intensity.

$$\Delta\text{OD} = -\log(\text{Norm Intensity}(t)).$$

Following the calculation of delta-optical density, two different principal component analysis (PCA) filters were applied to the data. The first PCA filter corrected for motion in the data, i.e., subject head movement. The second PCA filter used the principal components of the baseline data to project out systemic physiology. The resulting covariance reduced delta-optical density was used to calculate the change in concentration (delta concentration) from the modified Beer–Lambert law. For each of the two wavelengths, Lambda#1 = 780 nm and Lambda#2 = 805 nm, 2 simultaneous equations can be written to equate delta-optical density to oxygenated hemoglobin (HbO_2) and deoxygenated (Hb) concentration changes as below:

$$\Delta\text{ODLambda\#1} = \varepsilon_{\text{Hb}}^{\text{Lambda\#1}} * L * [Hb] + \varepsilon_{\text{HbO}_2}^{\text{Lambda\#1}} * L * [\text{HbO}_2]$$

$$\Delta\text{ODLambda\#2} = \varepsilon_{\text{Hb}}^{\text{Lambda\#2}} * L * [\text{Hb}] + \varepsilon_{\text{HbO}_2}^{\text{Lambda\#1}} * L * [\text{HbO}_2]$$

where ε is the molar absorption coefficient for Hb and HbO_2 at the two wavelengths specified and L is the optical path length. Solving the two equations obtains the concentration changes for oxygenated and deoxygenated hemoglobin:

$$\Delta\text{Hb}X = (e^T e)^{-1} e^T [\Delta\text{OD}].$$

We used a differential-pathlength factor of 6.0 and partial volume correction of 50, as can be set in the advanced filtering options of the toolbox. As the sampling rate for signal acquisition was 14 Hz, we obtained 140 delta concentration values, each for

oxygenated hemoglobin and deoxygenated hemoglobin, during a 10 s motor imagery task of each trial.

The data were then block averaged after specifying the pre- (5) and post-stimulus (140) time points for averaging, multiple stimulus conditions (1 for left-hand imagery, and 2 for right-hand imagery) and their timings. Block averaging was performed on each condition (left-hand and right-hand imagery) separately, first on a single run and later on across all data files. Statistical effects analysis based on analysis of variance (ANOVA) was conducted on the hemodynamic responses.

Following averaging, for each of the conditions (left-hand and right-hand imagery), images of hemodynamic activations superimposed on the probe geometry were constructed. Image reconstruction in HomER currently supports the back-projection methods and linear forward models created from semi-infinite (homogeneous) slab geometries. For details, please refer to the HomER User's Guide (available for public download and use at http://www.nmr.mgh.harvard.edu/PMI/). We used the following values for the image reconstruction constants in HomER: absorption and scattering coefficients (10 and 0.2), voxel dimensions (*Y*: 4.00:0.40:4.00, *X*: −4.00:0.65:9.00) and reconstruction depth (2:2:2). The results of the signal analysis will be discussed under the Results section.

Pattern classification

Pattern classification was performed on the raw signals obtained from the signal acquisition process after the signal preprocessing operations described below. We did not re-use the processed signals from the preliminary analysis (Preliminary signal

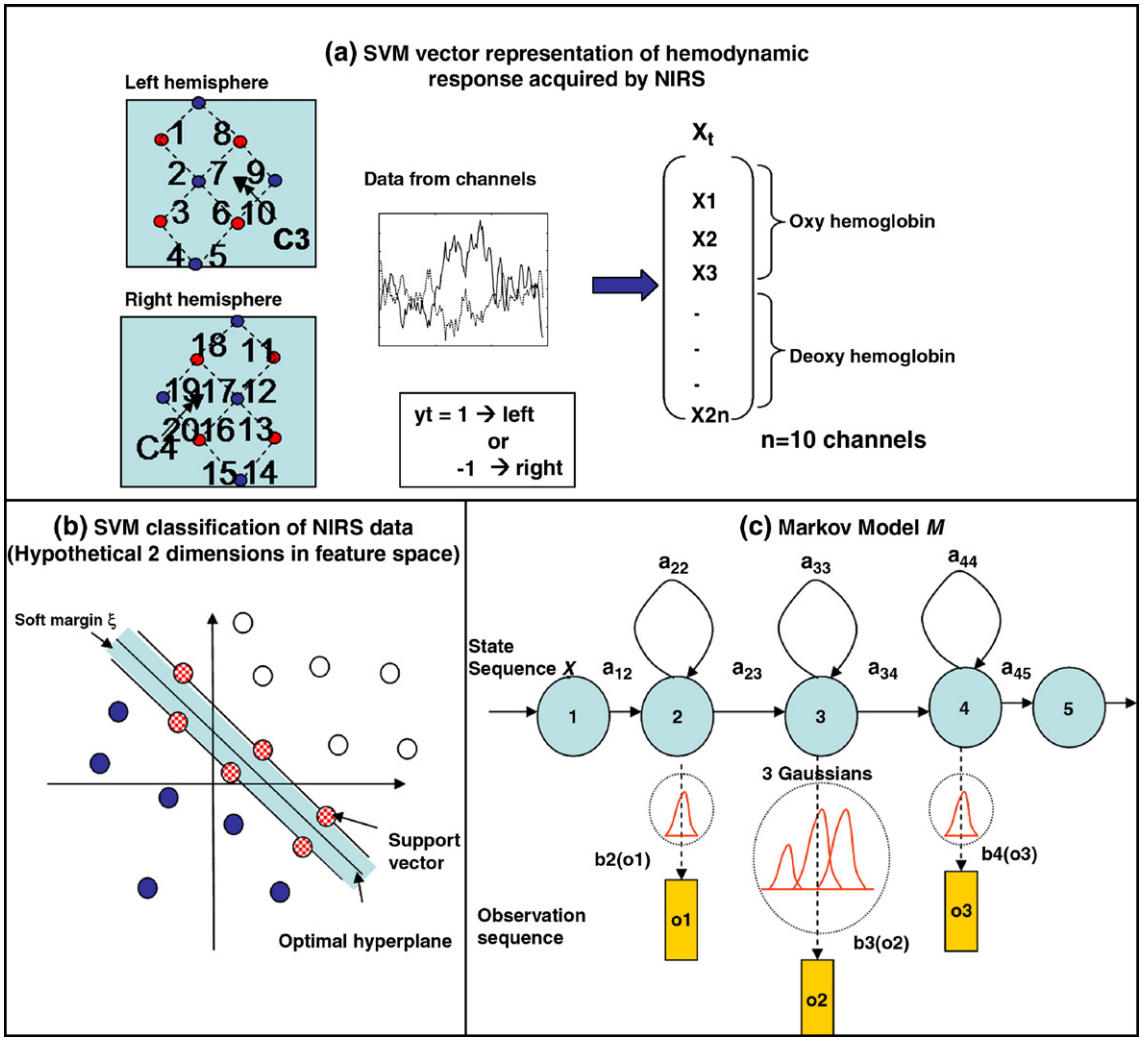

Fig. 2. (a) As input to the pattern classifier, a feature vector $\mathbf{X}_t$, containing the concentration values of the oxygenated hemoglobin and deoxygenated hemoglobin from the 20 channels of optodes from both hemisphere, was created for each trial duration of interest of the motor task (2–10 s in this case). For each trial period t, y_t represents the type of task the subject performed, for example, left-hand imagery (class = 1) and right-hand imagery (class = −1). (b) In the formulation of the SVM, the input feature vector is mapped to a high dimensional feature space through a non-linear transformation function. The SVM algorithm attempts to find a decision boundary or a separating hyperplane in the feature space. (c) Schematic diagram representing the HMM model for motor imagery. The HMM is designed as a left to right model, transitions being allowed from a state to itself and to any right neighbor state. Arrows from left to right indicate the allowed transitions of states. States 1 and 5 were *non-emitting*, meaning that they do not result in any observations. Observations 2 and 4 were modeled using a single Gaussian, while observation 3 was modeled using a mixture of 3 Gaussians.

analysis) for pattern classification as the intentions of the two methods were quite different. However, in the future, some of the artifact removal techniques used in HomER, such as principal component analysis (PCA) for head motion correction and systemic physiological changes, could be employed to potentially improve classification accuracy.

First, the acquired signals were processed to remove artifacts from heart beat and high frequency noise from muscle activity. We

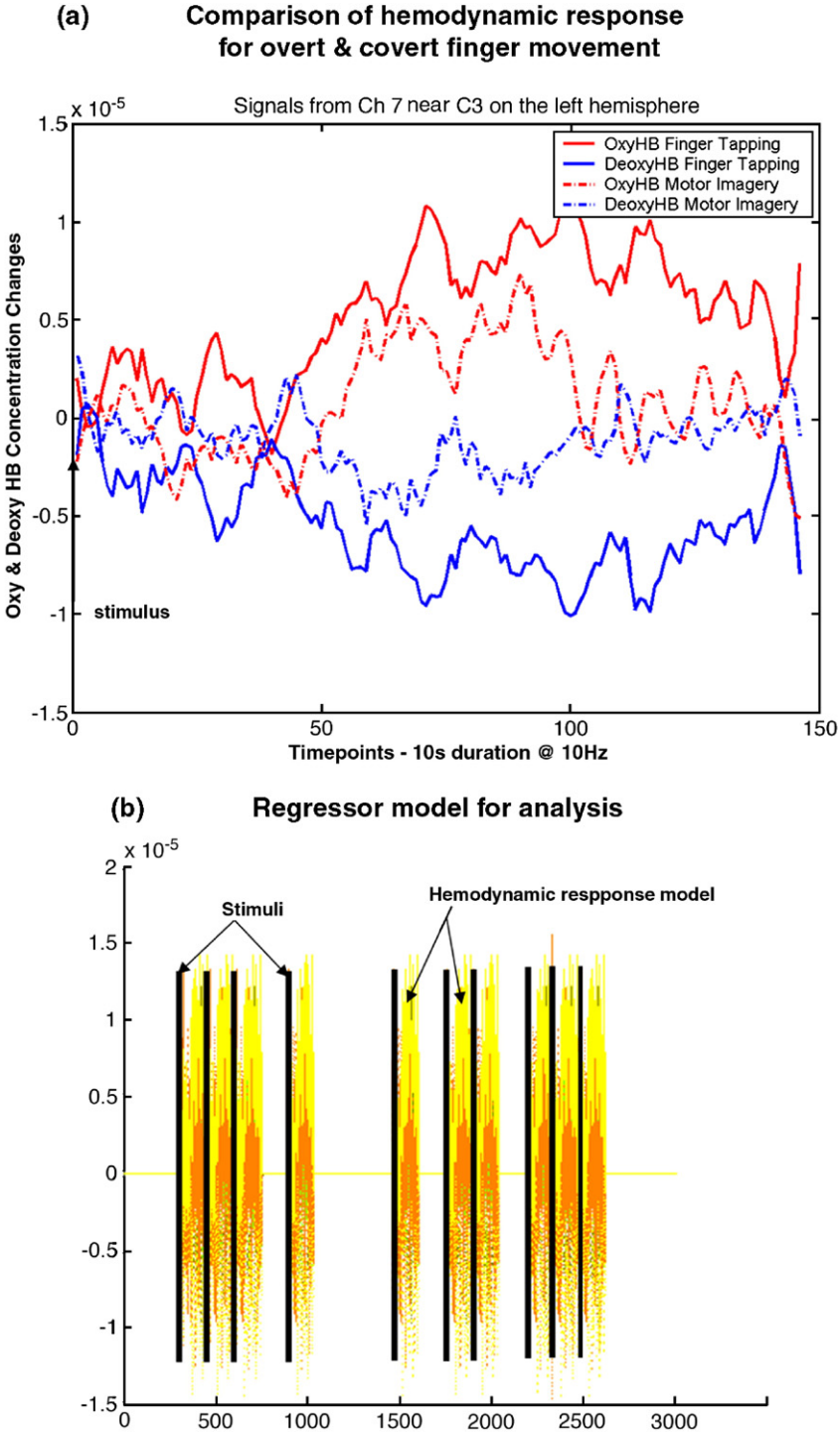

Fig. 3. (a) Exemplary data from Subject-1 performing right-hand finger tapping and motor imagery. Data displayed are averaged signals across a full session from channel 7 on the contralateral (left) hemisphere (close to the C3 electrode position as per the 10–20 system) for the duration 0–140 time points after stimulus presentation. Note that 140 time points are equal to 10 s of execution of the motor task at a sampling rate of 14 Hz. (b) Regressor model for right-hand motor imagery task, based on the timings of onset of stimuli for the task. The model was used for computing the analysis of variance (ANOVA) statistics and other measures in the HomER toolbox.

applied the Chebyshev type II filter (Parks and Burrus, 1987) that has a flat pass band, a moderate group delay, and an equiripple stop band. The filter was designed using "cheb2ord" and "cheby2" functions in Matlab (Mathworks, Inc., USA), using cut-off frequency at 0.7 Hz, stop frequency at 1 Hz, pass-band loss at no more than 6 dB and at least 50 dB of attenuation in the stop-band.

Time series of amplitude changes of oxygenated hemoglobin and deoxygenated hemoglobin in the period 2–10 s after stimulation for the motor task to start for each trial were extracted from the preprocessed data and fed to the pattern classification system. In the following subsections, we shall describe the implementation of two different pattern classification techniques, namely, Support Vector Machines and Hidden Markov Model.

Support Vector Machine (SVM)

The classification task is based on two separate sets of training data and testing data containing several instances of data. Each instance in the training set contains one *target value*, called the class label and several *attributes* or *features*. The goal of SVM is to produce a model which predicts target values in the testing set when only the attributes are given.

By formal notation, the classification problem involves determining a scalar class label y_t from a measurement vector $\mathbf{X}_t$. For classification of the NIRS data from multiple channels from both hemispheres, $\mathbf{X}_t$ represents the concentration values of oxygenated haemoglobin and deoxygenated haemoglobin from all the numbered channels (1–20) for the duration of the trial, specified by T ($1 \leq t \leq T$), and y_t is the experimental value of the task for that time (Fig. 2(a)). For each trial period t, y_t represents the type of task the subject was performing, for example, left-hand imagery (class = 1) and right-hand imagery (class = −1). During the experimental procedure for collecting training data, as the subject performs alternating trials of left-hand and right motor imagery, time series of preprocessed oxygenated and deoxygenated haemoglobin concentration changes are organized as a vector $\mathbf{X}_t$, and the class label y_t is marked as + or −1 according to the type of task. The present work is restricted to the binary classification problem ($y_t = \pm 1$).

In the formulation of the SVM, the input vector $\mathbf{X}_t$ is mapped to a high dimensional feature space, $\mathbf{Z}_t$, through a non-linear transformation function, $g(.)$ so that $\mathbf{Z}_t = g(\mathbf{X}_t)$. The SVM algorithm attempts to find a decision boundary or a separating hyperplane in the feature space, given by the decision function:

$$D(\mathbf{Z}_t) = (\mathbf{W} \cdot \mathbf{Z}) + w_0,$$

where $\mathbf{W}$ defines the linear decision boundaries (Fig. 2(b)). The solution $\mathbf{W}$ that represents the hyperplane can be obtained by solving for the equation:

$$y_t[(\mathbf{W} \cdot \mathbf{Z}) + w_0] \geq 1$$

The solution is optimal when $||\mathbf{W}||^2 + C \cdot f(\xi)$ is minimized under this constraint, where the parameter $C > 0$, termed the regularization constant, is chosen by the user. A large value of C corresponds to higher penalty for errors.

We implemented the SVM classifier using the LibSVM package (Chang and Lin, 2001). The LibSVM package is a C++ implementation, providing various features for SVM classification: C and v classification, one-class classification, ε and v regression; linear, polynomial, radial basis function and sigmoidal kernels; and v-fold cross-validation. Our implementation was carried out in the following steps:

(a) Transform the NIRS data into the format of the LibSVM software,
(b) Scale the data,
(c) Choose the type of kernel,
(d) Find the best penalty parameter and kernel parameters,
(e) Use the above parameters in the SVM model in 8 runs of 5-fold cross-validation to determine the classification accuracy.

The training and testing sets were created as vectors of real numbers of oxygenated and deoxygenated haemoglobin concentration values from the 20 channels for each trial of left-hand and right-hand motor imagery tasks, as shown in Fig. 2(a). The whole dataset was scaled before applying SVM. The main reason for scaling was to avoid attributes in greater numeric ranges from dominating those in smaller numeric ranges. As kernel values are obtained by the inner product of feature vectors, large attribute values may cause numerical problems. For these reasons, each attribute was scaled to a value in the range [−1, 1].

We used the linear kernel for the present study. We used the default value of 1 for the penalty parameter C as set in the LibSVM toolkit. Next, we performed a 5-fold cross-validation to determine the classification accuracy. The cross-validation procedure is also known to prevent the over-fitting problem. We conducted 8 runs of 5-fold cross-validation. In each run, the trials in the training dataset were randomly permutated and divided into 5 subsets of equal size. In each of the 5 folds, four subsets of data were used for training, while one subset was used for testing (validation) and the classification accuracy was calculated based on it. After 8 runs of 5-fold cross-validation, we obtained 40 test results (accuracy measures). We performed similar classification tests on overt finger tapping and covert motor imagery tasks, separately.

Hidden Markov Model

The HMM could be seen as a finite state automaton, containing s discrete states, emitting an observation vector (or output vector) at every time point that depends on the current state. Each observation vector is modeled using m Gaussian mixtures per state. The transition probabilities between states are defined using a transition matrix. The basic principles of HMM as applied to the NIRS signal classification problem will be discussed in this section. A detailed description of the method can be found in Rabiner (1989).

We used the Hidden Markov Model Toolkit (HTK) from the Department of Engineering of Cambridge University, United Kingdom for our implementation (Young et al., 1993). Written in ANSI C, HTK is an integrated suite of tools for building and manipulating continuous density HMMs.

Fig. 2(c) is a schematic diagram representing our HMM model for motor imagery. Left-hand and right-hand motor imagery were identically modeled as depicted, and the model parameters were subsequently estimated separately with respective data. We chose 5 states for the model based on previous HMM models for motor imagery classification (Obermaier et al., 2001) and our own preliminary experiments with modeling. The HMM is designed as a left to right model, transitions being allowed from a state to itself and to any right neighbor state. Arrows from left to right indicate the allowed transitions of states. States 1 and 5 were *non-emitting*, meaning that they do not result in any observations. Observations 2

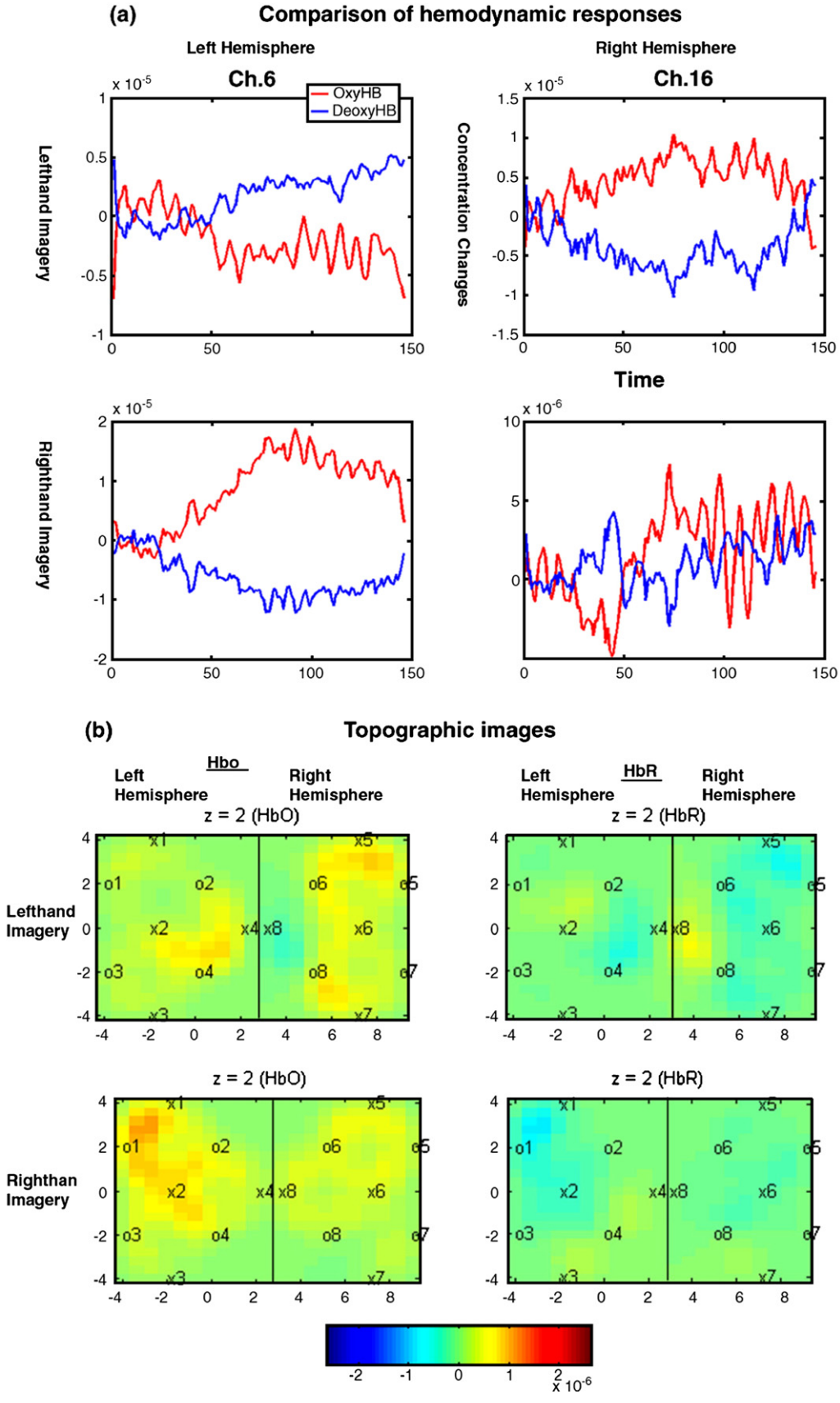
(a)
Comparison of hemodynamic responses
Left Hemisphere
Right Hemisphere
Ch.6
Ch.16
OxyHB
DeoxyHB
Lefthand Imagery
Righthand Imagery
Concentration Changes
Time
(b)
Topographic images
Hbo
HbR
Left Hemisphere
Right Hemisphere
z = 2 (HbO)
z = 2 (HbR)
Lefthand Imagery
Righthan Imagery

and 4 were modeled using a single Gaussian while observation 3 was modeled using a mixture of 3 Gaussians.

In this HMM model denoted by M, at each time t that a state j is entered, an observation vector $\mathbf{o}_t$ is generated from the probability density $b_j(o_t)$. Furthermore, transition from state i to state j is also probabilistic and is governed by the discrete probability a_{ij}. The joint probability O generated by the model M moving through the state sequence X is calculated as the product of transition probabilities and output probabilities. For the state sequence X in Fig. 2(c),

$$P(O|M) = a12b2(o1)a22b2(o1)a33b3(o2)\ldots$$

The observation O is known and the state sequence X is hidden. Given that X is unknown, the required likelihood is computed by summing over all possible state sequences $X=x(1),x(2),x(3),\ldots,$ $x(T)$, that is

$$P(O,X|M) = \sum_x a_{x(o)x(1)} \prod_{t=1}^{T} b_{x(t)}(o_t)a_{x(t)x(t+1)}$$

where $x(o)$ is constrained to the model entry state and $x(T+1)$ is constrained to the model exit state. Using the training samples for left-hand or right-hand motor imagery, the parameters $\{a_{ij}\}$ and $\{b_j(o_t)\}$ of the model for the respective task are determined by an estimation procedure. To determine the parameters of the HMM model, the HTK uses the Baum–Welch re-estimation procedure (Young et al., 1993). To recognize an unknown trial data, the likelihood of each model generating the trial data (observation vector) is calculated using the Viterbi algorithm (Rabiner, 1989, Rabiner and Juang, 1993), and the most likely model identifies the data as resulting from left-hand or right-hand task.

Our implementation of the HMM classifier comprised of the following steps:

(a) Transform the NIRS data into the format of the HTK software,
(b) Scale the data,
(c) Train 2 models of HMMs, one for left-hand task and one for right-hand task by computing the model parameters using the Baum–Welch re-estimation algorithm,
(d) Use the above models in 8 runs of 5-fold cross-validation to determine the classification accuracies.

The training and testing sets were created as vectors of real numbers of oxygenated and deoxygenated haemoglobin concentration values, as per the format expected by the HTK software, from the 20 channels for each trial of left-hand and right-hand motor imagery tasks. With 80 trial examples of each pattern, viz., single trial data of left-hand or right task, one HMM was trained for each type of task. For the purpose of comparison with SVM, we used the same evaluation methodology of 8 runs of 5-fold cross-validation. We performed similar classification tests on overt finger tapping and covert motor imagery tasks, separately.

Results

To start with, we wanted to check if overt finger tapping and covert motor imagery produced qualitatively similar responses. Fig. 3(a) shows exemplary data from Subject-1 performing right-hand finger tapping and motor imagery. Data displayed are averaged signals across a full session from channel 7 on the contralateral (left) hemisphere (close to the C3 electrode position as per the 10–20 system) for the duration 0–140 time points after stimulus presentation. Note that 140 time points are equal to 10 s of execution of the motor task at a sampling rate of 14 Hz. Typically, concentration of oxygenated hemoglobin (red lines) increased and concentration of deoxygenated hemoglobin (blue lines) decreased during both finger tapping (continuous lines) and motor imagery (dashed lines) tasks. However, changes in concentration, both for oxygenated hemoglobin and deoxygenated hemoglobin, for finger tapping were greater than those for motor imagery. Applying the analysis of variance (ANOVA) on the data based on the regressor model (Fig. 3(b)) in the HomER toolbox obtained significant activation for oxygenated and deoxygenated hemoglobin values, both for finger tapping and motor imagery, with $P<0.001$ and correlation coefficient $R^2=0.9$.

Next, we wanted to check if hemodynamic responses during motor imagery tasks in ipsilateral and contralateral hemispheres have substantial differences. Fig. 4(a) illustrates exemplary data for Subject-1, from channels on the left hemisphere and right hemisphere, while performing left-hand and right-hand motor imagery. Typically, most channels on the contralateral hemisphere showed activation by an increase in oxygenated hemoglobin and decrease in deoxygenated hemoglobin, while the channels on the ipsilateral hemisphere either showed similar response but to a smaller extent or in a reversed manner (increase in deoxygenated hemoglobin and decrease in oxygenated hemoglobin) potentially indicating inhibition.

Fig. 4(b) shows images reconstructed from the averaged hemodynamic responses from both left and right hemispheres while Subject-1 performed left-hand and right-hand motor imagery tasks. The reconstructed images for oxygenated hemoglobin and deoxygenated hemoglobin are superimposed on the probe geometry, with $x1$–$x8$ representing illuminator optodes and $o1$–$o8$ representing detector optodes. Activations are shown by yellow and red pixels and inhibitions by blue and green pixels. We found inter-subject variability in activation, illustrated by the variability between reconstructed images for different subjects.

The above analyses illustrated that there exist distinct patterns of hemodynamic responses as measured by NIRS to left-hand and right-hand motor imagery tasks which could be utilized in a pattern classifier towards developing a BCI. Table 1 lists the mean and standard deviation of accuracy of classification of left-hand motor task from right-hand motor task, using SVM and HMM techniques, on the data collected from 5 healthy volunteers. For the purpose of comparison, we classified both finger tapping and

Fig. 4. (a) Hemodynamic response during motor imagery tasks at the ipsilateral hemisphere has substantial difference from that of the contralateral hemisphere. Exemplary data of averaged oxygenated and deoxygenated concentration changes for Subject-1, from channels on the left hemisphere (Ch 6) and right hemisphere (Ch 16), while performing left-hand and right-hand motor imagery. Typically, channels on the contralateral hemisphere showed activation by an increase in oxygenated hemoglobin and decrease in deoxygenated hemoglobin, while the channels on the ipsilateral hemisphere either showed similar response but to a smaller extent or in a reversed manner (increase in deoxygenated hemoglobin and decrease in oxygenated hemoglobin) potentially indicating inhibition. (b) Exemplary topographic images from Subject-1. Images were reconstructed by back-projection methods and linear forward models in the HomER toolkit from the averaged hemodynamic responses from both left and right hemispheres while Subject-1 performed left-hand and right-hand motor imagery tasks. The reconstructed images for oxygenated hemoglobin and deoxygenated hemoglobin are superimposed on the probe geometry, with $x1$–$x8$ representing illuminator optodes and $o1$–$o8$ representing detector optodes.

Table 1
Accuracy of Support Vector Machine (SVM) and Hidden Markov Model (HMM) classification of finger tapping and motor imagery tasks for 5 healthy volunteers

Subject	% Accuracy BY SVM (avg~STD)		% Accuracy BY HMM (avg~STD)	
	Finger tapping	Motor imagery	Finger tapping	Motor imagery
Subject-1	94.27 ~ 4.99	75.62 ~ 3.42	94.76 ~ 3.01	91.29 ~ 8.88
Subject-2	78.44 ~ 10.31	69.84 ~ 8.23	91.44 ~ 8.71	89.7 ~ 8.58
Subject-3	79.37 ~ 10.85	71.45 ~ 8.11	92.78 ~ 4.93	91.76 ~ 6.53
Subject-4	93.81 ~ 5.63	74.87 ~ 3.56	93.83 ~ 4.94	79.14 ~ 12.36
Subject-5	91.68 ~ 8.15	73.94 ~ 7.45	94.43 ~ 5.41	93.76 ~ 5.95
Total	87.5	73.1	93.4	89.1

motor imagery data, although the proposed BCI was intended to be operated by motor imagery alone.

Finger tapping data were classified with better accuracy compared to motor imagery data by both classification techniques for all the subjects. Average accuracy of classification across all the subjects for finger tapping, by SVM and HMM, was 87.5% and 93.4%, respectively, as against 73.1% and 89.1% for motor imagery. Between the two pattern classification techniques, HMM performed better than SVM for both finger tapping and motor imagery tasks. The accuracy of classification by HMM in comparison to SVM was greater by 5.9% for finger tapping, while the improvement was a striking 16% for motor imagery.

Discussion

Preliminary analysis of the NIRS signals collected during left-hand and right-hand motor imagery tasks indicated variation of the profile of the oxygenated and deoxygenated concentration changes from trial to trial. The dynamic nature of the signal could be due to inconsistency in the execution of motor imagery, especially when performed without any form of feedback. During overt finger tapping, the subject gets somatosensory and visual feedback of his/her own movement, while this is not so for the motor imagery task. A subject may start an imagination task at a different point in time in each trial. Furthermore, he may perform the imagination at different tempos in different trials, creating considerable difficulties to the pattern recognition of the signal. This could be one of the reasons for the higher classification accuracy of finger tapping compared to motor imagery for both the classification techniques (SVM and HMM). With this consideration, we anticipated that a probability network like the HMM might model the dynamic nature of the hemodynamic time series more effectively. Interestingly, this was confirmed by the greater improvement in classification accuracy by HMM for motor imagery (16% increase) compared to the improvement in accuracy for finger tapping (5.9% increase). Recently, Zhang and Guan (2006) developed an improved method to address the above variations in the NIRS signal in response to motor imagery. The proposed technique uses a kernel-based model to represent variations in the hemodynamic signals of interest. Furthermore, a mathematical procedure was developed to locate the signals by estimating the parameters of the model. SVM was used on the located signals to differentiate left-hand imagery from right-hand imagery. The authors validated the method on simulated data as well as real data to obtain an error reduction of as much as 13%. This method can be potentially employed with HMM to improve classification accuracy even further.

By foregone results, we have established that there exist distinct patterns of hemodynamic responses between left-hand and right-hand imagery and that such patterns can indeed be classified offline with substantially greater than chance accuracy. Our results of high accuracy of offline pattern classification of NIRS signals during motor imagery tasks, especially with the HMM classifier, indicate the potential use of such techniques to the further development of an online BCI system. Towards this end, we have implemented an NIRS–BCI system incorporating a word speller as a language support system for the disabled, as shown in Fig. 5. The system is written as a stand-alone application in C/C++, with C# used for development of the graphical user interface (GUI). The system comprises of four online modules: signal acquisition, signal processing, signal classification and word speller application with online feedback to the user. The signal acquisition module currently supports real-time data acquisition from 2 commercially available NIRS systems: OMM-1000 (Shimadzu Corporation, Japan) and Imagent System (ISS Inc., USA), through a serial port connection and two pluggable software components to support the differences in the data formats of the two instruments. The signal processing module implements low and high pass filtering and temporal smoothing. The pattern classification module currently supports SVM and HMM techniques. The SVM classifier is based on the LibSVM C++ library (Chang and Lin), while the HMM classifier is based on the HTK library (Young et al., 1993). The word speller interface provides a means to use NIRS responses created by left- and right-hand motor imagery to spell words by a 2-choice cursor control paradigm. The user has to use left- or right-hand imagery to move the cursor to the left or right respectively to select a box that contains the letter of choice. Feature vectors of oxygenated and deoxygenated hemoglobin values from all channels in a moving window of 4 s are used as input to the pattern classifier. The length of the moving window can be increased or decreased depending on the performance requirements of execution and the expertise of the user. In terms of operation, the word speller is quite similar to the language support system of the Thought Translation Device (TTD) (Birbaumer et al., 1999, 2000).

A suitable training protocol needs to be developed to extend the offline pattern classification system to an active, online BCI system that drives the word speller application. In this regard, a 2-step procedure is being used. First, for each subject, parameters of the classifier (SVM or HMM) are estimated during offline training and stored as a subject-specific model. This is necessary, as we have seen that there is a great deal of variability between subjects in their hemodynamic response patterns. Next, subject-specific model parameters are loaded as the initial parameters of the classifier for online training. During online training on the word speller, the subject uses motor imagery to learn to control the cursor for selection of letters. At the end of each online training session, his model parameters are re-estimated based on the newly acquired

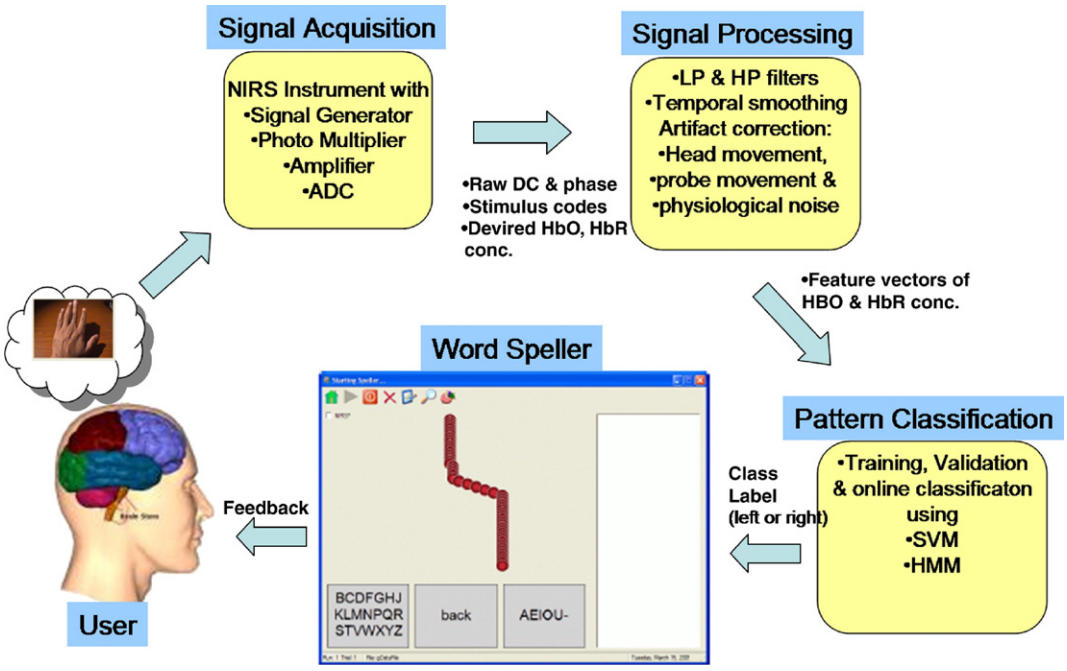

Fig. 5. Architecture of the near-infrared spectroscopy BCI (NIRS–BCI). Multichannel NIRS signals from both hemispheres are acquired in real time, processed, classified online by either a Support Vector Machine (SVM) or a Hidden Markov Model (HMM) and translated for driving the word speller application.

data. This way, with each new training session, the BCI would be re-tuned to operate in an online mode.

Until now, we have only considered a 2-choice BCI system operated by classifying left-hand and right-hand motor imagery. Potentially, such a system can be extended to 3- or 4-choice operation by imagery of the legs, and simultaneous imagery of hands and legs. Furthermore, other paradigms of BCI control, such as the P300 hemodynamic response, could also be explored. Kennan et al. (2002) reported simultaneous recording of event-related auditory oddball (P300) response using NIRS and surface EEG. A peak signal of oxygenated hemoglobin was observed around 6 s after the onset of the oddball stimulus. Many other studies that assessed motor and cognitive functions using NIRS (Hoshi and Tamura, 1993, 1997; Kato et al., 1993; Kleinschmidt et al., 1996; Okada et al., 1997; Hoshi et al., 2000, 2001) may indicate how future BCIs could be developed.

A major drawback of NIRS is the long time constants of the hemodynamic response making NIRS–BCI potentially very slow to operate. A fast NIRS signal (Wolf et al., 2002, 2003a, 2003b) is reported to appear in the range of milliseconds after stimulation. The signal is generated by rapid changes in the optical properties of the cerebral tissue. These changes presumably are due to an alteration of the scattering properties of neuronal membranes, which occur simultaneously with electrical changes, cell swelling and increased heat production. Thus, the fast signal is believed to be directly related to neuronal activity, as EEG or MEG, in contrast to functional NIRS, fMRI (BOLD signal) and PET detecting only the slow hemodynamic response to neuronal activity. However, the fast signal is more difficult to detect because the optical changes are small and other physiological signals, such as the hemodynamic pulsativity due to the heart beat, dominate. Therefore, the system has to be highly noise resistant. Many trials of the fast signal need to be averaged to improve signal-to-noise ratio. When the above limitations and problems have been sufficiently overcome, the fast signal could prove beneficial to BCI development.

In this study, we have demonstrated the feasibility of a BCI using near-infrared spectroscopy. Further work needs to be carried out to develop and test an online BCI system for the disabled. Novel signal processing methods need to be developed to exploit the NIRS signal. NIRS avoids the noise prominent in the electrical signals. It is less cumbersome to use as there is no need to apply conductive gel. NIRS is non-ionizing, and so suitable for long-term use. However, NIRS also has certain drawbacks. It is slow to operate because of the inherent latency of the hemodynamic response. The signal strength is affected by hair on the head (especially if the subject has thick dark hair). Furthermore, if the probes are not secured well, the relative motion of the optodes on the hair may introduce motion artifacts and drifts in the hemodynamic signal. In spite of these limitations, NIRS' ability to localize brain activity 1–3 cm below the surface of cortex, with a spatial resolution in the range of centimeters, could be an advantage in BCI development. NIRS provides us with an excellent opportunity to use a variety of motor and cognitive activities to detect signals from specific regions of the cortex for the development of future BCIs.

Acknowledgments

This work is being carried out as a collaborative research project among four organizations, namely, Institute for Infocomm Research, Singapore; Tokyo Institute of Psychiatry, Japan; Medical Systems Department of Shimadzu Corporation, Japan; and the Institute for Medical Psychology and Behavioral Neurobiology of the University of Tuebingen, Germany. Authors R.S. and N.B. are supported by the Deutsche Forschungsgemeinschaft (DFG) and the National Institute of Health (NIH). We are grateful to the

developers of LibSVM, HMM and HomER toolkits for allowing us to use their software in our work. We would like to thank our colleagues Ahmed Karim and Ralf Veit for helpful comments on the manuscript.

References

Beisteiner, R., Hollinger, P., Lindinger, G., Lang, W., Berthoz, A., 1995. Mental representation of movements. Brain potentials associated with imagination of hand movements. Electroencephalogr. Clin. Neurophysiol. 183–193.

Benaron, D.A., Hintz, S.R., Villringer, A., Boas, D., Kleinschmidt, A., Frahm, J., Hirth, C., Obrig, H., van Houten, J.C., Kermit, E.L., Cheong, W.F., Stevenson, D.K., 2000. Noninvasive functional imaging of human brain using light. J. Cereb. Blood Flow Metab. 20, 469–477.

Birbaumer, N., 2006. Brain–computer-interface research: coming of age. Clin. Neurophysiol. 117, 479–483.

Birbaumer, N., Ghanayim, N., Hinterberger, T., Iversen, I., Kotchoubey, B., Kubler, A., Perelmouter, J., Taub, E., Flor, H., 1999. A spelling device for the paralysed. Nature 398, 297–298.

Birbaumer, N., Kubler, A., Ghanayim, N., Hinterberger, T., Perelmouter, J., Kaiser, J., Iversen, I., Kotchoubey, B., Neumann, N., Flor, H., 2000. The thought translation device (TTD) for completely paralyzed patients. IEEE Trans. Rehabil. Eng. 8, 190–193.

Birbaumer, N., Hinterberger, T., Kubler, A., Neumann, N., 2003. The thought-translation device (TTD): neurobehavioral mechanisms and clinical outcome. IEEE Trans. Neural Syst. Rehabil. Eng. 11, 120–123.

Blankertz, B., Curio, G., Muller, K., 2001. Classifying Single Trail EEG: Toward Brain Computer Interfacing. MIT Press, Cambridge, MA.

Chang, C.C., Lin, C.J., 2001. LIBSVM—A Library for Support Vector Machines. http://www.csie.ntu.edu.tw/cjlin/libsvm/.

Coyle, S., Ward, T., Markham, C., McDarby, G., 2004. On the suitability of near-infrared (NIR) systems for next-generation brain–computer interfaces. Physiol. Meas. 25, 815–822.

Delpy, D.T., Cope, M., van der Zee, P., Arridge, S., Wray, S., Wyatt, J., 1988. Estimation of optical pathlength through tissue from direct time of flight measurement. Phys. Med. Biol. 33, 1433–1442.

Hoshi, Y., Tamura, M., 1993. Dynamic multichannel near-infrared optical imaging of human brain activity. J. Appl. Physiol. 75, 1842–1846.

Hoshi, Y., Tamura, M., 1997. Near-infrared optical detection of sequential brain activation in the prefrontal cortex during mental tasks. NeuroImage 5, 292–297.

Hoshi, Y., Oda, I., Wada, Y., Ito, Y., Yutaka, Y., Oda, M., Ohta, K., Yamada, Y., Mamoru, T., 2000. Visuospatial imagery is a fruitful strategy for the digit span backward task: a study with near-infrared optical tomography. Brain Res. Cogn. Brain Res. 9, 339–342.

Hoshi, Y., Kobayashi, N., Tamura, M., 2001. Interpretation of near-infrared spectroscopy signals: a study with a newly developed perfused rat brain model. J. Appl. Physiol. 90, 1657–1662.

Kato, T., Kamei, A., Takashima, S., Ozaki, T., 1993. Human visual cortical function during photic stimulation monitoring by means of near-infrared spectroscopy. J. Cereb. Blood Flow Metab. 13, 516–520.

Kennan, R.P., Horovitz, S.G., Maki, A., Yamashita, Y., Koizumi, H., Gore, J.C., 2002. Simultaneous recording of event-related auditory oddball response using transcranial near infrared optical topography and surface EEG. NeuroImage 16, 587–592.

Kleinschmidt, A., Obrig, H., Requardt, M., Merboldt, K.D., Dirnagl, U., Villringer, A., Frahm, J., 1996. Simultaneous recording of cerebral blood oxygenation changes during human brain activation by magnetic resonance imaging and near-infrared spectroscopy. J. Cereb. Blood Flow Metab. 16, 817–826.

Obermaier, B., Guger, C., Pfurtscheller, G., 1999. Hidden Markov models used for the offline classification of EEG data. Biomed. Tech. (Berl.) 44, 158–162.

Obermaier, B., Guger, C., Neuper, C., Pfurtscheller, G., 2001. Hidden Markov models for online classification of single trial EEG data. Pattern Recogn. Lett. 1299–1309.

Okada, M., Firbank, M., Schweiger, S., Arridge, M., Delpy, C.D., 1997. Theoretical and experimental investigation of the near-infrared light propagation in a model of the adult head. Appl. Opt. 36, 21–31.

Parks, T.W., Burrus, C.S., 1987. Digital Filter Design. John Wiley and Sons, New York.

Pfurtscheller, G., Neuper, C., Schlogl, A., Lugger, K., 1998. Separability of EEG signals recorded during right and left motor imagery using adaptive autoregressive parameters. IEEE Trans. Rehabil. Eng. 6, 316–325.

Pfurtscheller, G., Neuper, C., Guger, C., Harkam, W., Ramoser, H., Schlogl, A., Obermaier, B., Pregenzer, M., 2000. Current trends in Graz Brain–computer Interface (BCI) research. IEEE Trans. Rehabil. Eng. 8, 216–219.

Pfurtscheller, G., Brunner, C., Schlogl, A., Lopes da Silva, F.H., 2006. Mu rhythm (de)synchronization and EEG single-trial classification of different motor imagery tasks. NeuroImage 31, 153–159.

Rabiner, L.R., 1989. A tutorial on hidden Markov models and selected applications in speech recognition. Proc. I.E.E.E. 77, 257–286.

Rabiner, L., Juang, B.H., 1993. Fundamentals of Speech Recognition. Prentice-Hall, Englewood Cliffs, NJ.

Serruya, M.D., Hatsopoulos, N.G., Paninski, L., Fellows, M.R., Donoghue, J.P., 2002. Instant neural control of a movement signal. Nature 416, 141–142.

Sitaram, R., Hoshi, Y., Guan, C. (Eds.), 2005. Near Infrared Spectroscopy based Brain–Computer Interface, vol. 5852.

Vapnik, V.N., 1998. Statistical Learning Theory. Wiley, New York.

Villringer, A., Obrig, H., 2002. Near Infrared Spectroscopy and Imaging. Elsevier Science, USA.

Weiskopf, N., Veit, R., Erb, M., Mathiak, K., Grodd, W., Goebel, R., Birbaumer, N., 2003. Physiological self-regulation of regional brain activity using real-time functional magnetic resonance imaging (fMRI): methodology and exemplary data. NeuroImage 19, 577–586.

Weiskopf, N., Mathiak, K., Bock, S.W., Scharnowski, F., Veit, R., Grodd, W., Goebel, R., Birbaumer, N., 2004a. Principles of a brain–computer interface (BCI) based on real-time functional magnetic resonance imaging (fMRI). IEEE Trans. Biomed. Eng. 51, 966–970.

Weiskopf, N., Scharnowski, F., Veit, R., Goebel, R., Birbaumer, N., Mathiak, K., 2004b. Self-regulation of local brain activity using real-time functional magnetic resonance imaging (fMRI). J. Physiol. (Paris) 98, 357–373.

Wolf, M., Wolf, U., Choi, J.H., Gupta, R., Safonova, L.P., Paunescu, L.A., Michalos, A., Gratton, E., 2002. Functional frequency-domain near-infrared spectroscopy detects fast neuronal signal in the motor cortex. NeuroImage 17, 1868–1875.

Wolf, M., Wolf, U., Choi, J.H., Gupta, R., Safonova, L.P., Paunescu, L.A., Michalos, A., Gratton, E., 2003a. Detection of the fast neuronal signal on the motor cortex using functional frequency domain near infrared spectroscopy. Adv. Exp. Med. Biol. 510, 193–197.

Wolf, M., Wolf, U., Choi, J.H., Toronov, V., Paunescu, L.A., Michalos, A., Gratton, E., 2003b. Fast cerebral functional signal in the 100-ms range detected in the visual cortex by frequency-domain near-infrared spectrophotometry. Psychophysiology 40, 521–528.

Wolpaw, J.R., 2004. Brain–computer interfaces (BCIs) for communication and control: a mini-review. Clin. Neurophysiol., Suppl. 57, 607–613.

Wolpaw, J.R., McFarland, D.J., 2004. Control of a two-dimensional movement signal by a noninvasive brain–computer interface in humans. Proc. Natl. Acad. Sci. U. S. A. 101, 17849–17854.

Wolpaw, J.R., Birbaumer, N., Heetderks, W.J., McFarland, D.J., Peckham, P.H., Schalk, G., Donchin, E., Quatrano, L.A., Robinson, C.J., Vaughan, T.M., 2000a. Brain–computer interface technology: a

review of the first international meeting. IEEE Trans. Rehabil. Eng. 8, 164–173.

Wolpaw, J.R., McFarland, D.J., Vaughan, T.M., 2000b. Brain–computer interface research at the Wadsworth Center. IEEE Trans. Rehabil. Eng. 8, 222–226.

Wolpaw, J.R., Birbaumer, N., McFarland, D.J., Pfurtscheller, G., Vaughan, T.M., 2002. Brain–computer interfaces for communication and control. Clin. Neurophysiol. 113, 767–791.

Wolpaw, J.R., Loeb, G.E., Allison, B.Z., Donchin, E., do Nascimento, O.F., Heetderks, W.J., Nijboer, F., Shain, W.G., Turner, J.N., 2006. BCI meeting 2005—Workshop on signals and recording methods. IEEE Trans. Neural Syst. Rehabil. Eng. 14, 138–141.

Young, S.J., Woodland, P.C., Byrne, W.J., 1993. HTK Version 1.5: User, Reference and Programmer Manual. Entropic Research Laboratories, Washington, DC.

Zhang, H., Guan, C., 2006. Kernel-based signal localization method for NIRS brain–computer interfaces. Proceedings of the International Conference on Pattern Recognition, Hong Kong.